Magneto-optical properties of ferromagnetic/nonferromagnetic interfaces: Application to Co/Au(111)

J. Hamrle
Institute of Physics, Charles University, Ke Karlovu 5, 12116 Praha 2, Czech Republic
and Laboratoire de Physique des Solides, UMR CNRS 8502, Université Paris XI, 91405 Orsay, France

M. Nývlt,* Š. Višňovský, and R. Urban
Institute of Physics, Charles University, Ke Karlovu 5, 12116 Praha 2, Czech Republic

P. Beauvillain and R. Mégy
Institut d'Electronique Fondamentale, UMR CNRS 8622, Université Paris XI, 91405 Orsay, France

J. Ferré† and L. Polerecký
Laboratoire de Physique des Solides, UMR CNRS 8502, Université Paris XI, 91405 Orsay, France

D. Renard
Institute d'Optique Théorique et Appliquée, UMR CNRS 8501, Université Paris XI, 91405 Orsay, France
(Received 16 March 2001; revised manuscript received 12 June 2001; published 20 September 2001)

An approach is proposed to give a reliable description of the ferromagnetic/nonferromagnetic interface contributions to magneto-optical (MO) Kerr effect. We show that well chosen magneto-optical parameters related to the interfaces and extracted from the experimental data are independent on the angle of incidence and the polarization of the incident light. They are also invariant with respect to the optical properties and thicknesses of sandwiching layers. The method was tested on the Au/Co/Au(111) system. It was found that the assumptions and predictions of the theoretical description agree with the experimental observations. Further analysis of the experimental data shows indirectly that a significant part of the MO interface-induced effects are coming from the electronic hybridization at Au/Co interfaces. Consequently, the data could be a useful source of information for *ab initio* calculations of the layer-resolved permittivity tensor.

DOI: 10.1103/PhysRevB.64.155405 PACS number(s): 75.70.Cn, 78.68.+m, 78.20.Ls, 78.66.Bz

I. INTRODUCTION

Interfaces between ferromagnetic (FM) and nonferromagnetic metals attract considerable attention in the field of thin film magnetism. When the thickness of a magnetic film is substantially reduced (in the order of a few atomic layers), the interface effects become more significant or often control a lot of physical effects. This may even lead to new properties which are not observed in bulk materials, such as interface magnetic anisotropy. This anisotropy can overcome the demagnetizing field effects and give rise to an out-of-plane easy magnetization axis[1–3] or control spin reorientation transitions.[4] Hence, they play a significant role in artificial superlattices and have a fundamental importance in practical applications, such as perpendicular magneto-optical recording,[5] giant magnetoresistance sensors,[6] and random access memories.[7]

The interface anisotropy is mainly of electronic origin and primarily related to the spin-orbit coupling interaction from which originate magneto-optical (MO) effects. One therefore obviously expects that such interface effects should also modify MO properties of magnetic multilayer systems.

The most common MO effect used in the investigation of magnetic thin layers is the MO Kerr effect in light reflection.[4,8] Its magnitude is determined by the sum of individual contributions of all magnetic layers in a stratified structure. Consequently, in magnetic film structures, the Kerr effect includes also contributions originating from the interfaces. When the thickness of a magnetic film is reduced down to a few monoatomic layers, the interface contributions become easily detectable. These contributions can provide important information about the nature of the FM/non-FM electronic interactions. A typical example is the Pt/Co system, where due to Pt-Co hybridization, an electronic transition was observed in the polar Kerr effect spectra measured on multilayers[9,10] or Pt-Co alloy films.[11,12]

The change of electronic structure at the FM/non-FM interface can be interpreted by *ab initio* calculations. In principle, there are two possible approaches to the problem of the electronic interactions in multilayers. In the first approach, the periodic multilayer structure is considered as an artificial superlattice, i.e., as a new bulk material. This approach has been satisfactorily applied to Cu/Co,[13] Pd/Co,[14] and Au/Fe(001) (Ref. 15) superlattices. Although this is quite straightforward and elegant method, it does not provide spatially resolved information about the electronic interactions at the FM/non-FM interfaces.

The second approach introduces interface interlayers. In this case the multilayer stacking is always considered, but the sharp interfaces between the FM and non-FM materials are substituted by some very thin interface layers. This approach allows for a description of the FM/non-FM interface hybridization, strains, effects of stray fields, interface roughness or alloying, etc. Due to a rapid progress in the *ab initio*

 ©2001 The American Physical Society

calculations, the interface interlayer approach is even more fruitful than originally expected. A fully relativistic formalism has recently been developed by Huhne and Ebert[16] to define a layer-resolved frequency-dependent optical conductivity tensor in arbitrary layered systems. It can therefore be expected that in the very near future it will be possible to make a direct link between the microscopic *ab initio* calculations and the phenomenological interface interlayer models.

From the experimental point of view, the interface effects can be better studied on simple systems with one or two magnetic layers, because the structural properties can be better controlled. Such simple systems allowed recently a large progress in understanding of magnetic[17] and quantum size effects[18,19] in structures consisting of FM and noble metal layers. However, little attention has been paid to the MO properties of the FM/noble metal interface itself. This is due to the fact that up to now there was no technique available for separation of the pure MO characteristics of interfaces from the experimental MO data.

Until recently, the interface contribution was deduced from the analysis of the Kerr effect variation with the FM film thickness. As expected, both the theoretical models and experiments show that, if one neglects contributions from the non-FM layers, there is zero Kerr effect for zero thickness of the FM film. On the other hand, there is an experimental evidence that the *extrapolation* of the Kerr effect for zero FM film thickness is nonzero. This was observed, for example, in the Au/Co/Au sandwich structures[20] and in the Pd/Co/Pd (Ref. 21) and Pt/Co/Pt (Ref. 22) wedges. The nonzero extrapolation was assigned to the contribution of the FM/non-FM interface.

The interface contribution, for a given wavelength, depends upon several parameters, such as the angle of incidence, the incident light polarization, optical properties and thicknesses of the sandwiching layers, etc. Consequently, it is not straightforward to interpret the experimental MO data. In principle, it *is* possible to obtain MO properties of the interface interlayers by, e.g., fitting the experimental data to a theoretical model.[23] However, this is in most cases almost impossible as it requires the knowledge of optical parameters of *all* other layers involved in the multilayer system.

In this article we extend the analysis of the Kerr effect variation with the FM film thickness. We introduce a quantity which describes the MO properties of the FM/non-FM interface and can be deduced straightforwardly from the experimental data. It is demonstrated that this quantity is independent on the incidence angle of incoming light, its polarization (s or p) and the thicknesses and the optical parameters of sandwiching layers. Provided that the off-diagonal permittivity elements of the inner part of the ferromagnetic layer are known, this quantity can be used for evaluating the off-diagonal elements of the permittivity tensor of the interface interlayer. Furthermore, the technique can be used both for polar and longitudinal geometries of the multilayer magnetization.

The article is organized as follows. In Sec. II we shortly summarize analytical formulas giving the description of the Kerr effect in structures containing ultrathin magnetic films. In Sec. III we introduce integral MO characteristics of the structure which are subsequently used to derive a relation between the optical parameters and experimental characteristics of the FM/non-FM interface. Section IV summarizes sample properties and experimental procedures conducted to obtain the interface contributions to the total Kerr effect. The experimental data and the MO parameters of the interface interlayers are presented in Sec. V. Finally, simple models describing the contributions of the FM/non-FM interface to the MO Kerr effect are discussed in Sec. VI.

II. EXPERIMENTAL POLAR KERR EFFECT IN A SANDWICH STRUCTURE AND ITS REALISTIC ANALYTICAL DESCRIPTION

As follows from the experiment, the complex Kerr effect Φ can, to some extent, be described by a linear function of the FM film thickness $t^{(\mathrm{F})}$, i.e., $\Phi \sim B t^{(\mathrm{F})}$, where B is a complex number. The exact linearity is predicted by simplified models[8,24–27] which are derived under the following assumptions. (i) The optical profile of the multilayer structure is steplike, i.e., all layers are optically homogeneous and separated by sharp planar interfaces. (ii) The FM film is ultrathin, i.e., its thickness is assumed to be $t^{(\mathrm{F})} \ll \lambda/(4\pi|N^{(\mathrm{F})}|)$, where $N^{(\mathrm{F})}$ is the complex refractive index of the FM film and λ is the vacuum wavelength of the probing light. For example, at $\lambda = 300$ nm, the thickness of an ultrathin Co film ($|N^{(\mathrm{F})}| \approx 2.7$) has to be $t^{(\mathrm{F})} \ll 9$ nm. Because conditions (i) and (ii) are not completely fulfilled in real structures, the linear expression of Φ has to be corrected by a constant and a quadratic correction term, i.e.,

$$\Phi(t^{(\mathrm{F})}) = A + B t^{(\mathrm{F})} + C (t^{(\mathrm{F})})^2. \tag{1}$$

The coefficients A, B, and C are, in general, complex numbers. The term A accounts for the fact that the actual profile of the off-diagonal element of the permittivity tensor is not described by a steplike function of the coordinate across the multilayer system. The quadratic term is mainly related to the change of the diagonal reflection coefficients r_{ss}, r_{pp} with the FM layer thickness.[8,24]

In the following we will consider the polar Kerr effect, the magnetization of the FM layer being assumed perpendicular to the sample surface, i.e., $\vec{M} = (0,0,M_z)$. The MO properties of such a FM layer are described by the permittivity tensor

$$\boldsymbol{\varepsilon}^{(\mathrm{F})} = \begin{pmatrix} \varepsilon_0^{(\mathrm{F})} & -i\varepsilon_1^{(\mathrm{F})} & 0 \\ i\varepsilon_1^{(\mathrm{F})} & \varepsilon_0^{(\mathrm{F})} & 0 \\ 0 & 0 & \varepsilon_0^{(\mathrm{F})} \end{pmatrix}. \tag{2}$$

The diagonal elements $\varepsilon_0^{(\mathrm{F})}$ are assumed to be equal. These elements have only a small influence on the polar Kerr effect originating from the ultrathin magnetic layer, as will be demonstrated below.

For an ideal sandwich structure consisting of an homogeneous *ultrathin* FM layer of thickness $t^{(\mathrm{F})}$, the linear polar Kerr effect[8,25,26] is proportional to the off-diagonal element $\varepsilon_1^{(\mathrm{F})}$ of the permittivity tensor (2), i.e.,

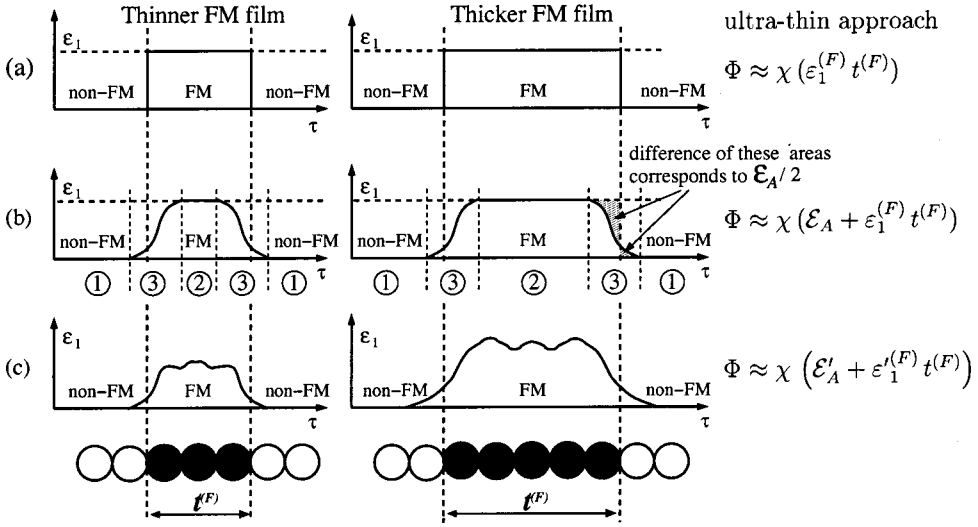

FIG. 1. Schematic representation of three different profiles $\varepsilon_1(\tau)$ of the off-diagonal optical permittivity tensor elements in a sandwich non-FM/FM/non-FM structure. Case (a) represents the simplest steplike profile for which the Kerr effect Φ is proportional to $t^{(F)}$. In case (b) the off-diagonal permittivity changes gradually in the non-FM/FM interface regions 3 and stays constant in the inner parts 2 of the FM layer. Case (c) represents a general profile $\varepsilon_1(\tau)$.

$$\Phi = \chi \varepsilon_1^{(F)} t^{(F)} = \chi \mathcal{E}. \tag{3}$$

In the following, we will refer to the off-diagonal element $\varepsilon_1^{(F)}$ as the *off-diagonal permittivity*. Similarly, the coefficient $\mathcal{E}$, which stands for the product $\varepsilon_1^{(F)} t^{(F)}$, will be referred to as the *integral off-diagonal permittivity*.

The terms $\mathcal{E}$ and χ are related to the properties of the ultrathin FM layer itself and the optical properties of the rest of the sandwiching layers, respectively. If the ultrathin FM layer is deposited on a semi-infinite non-FM substrate and covered by a non-FM overlayer of the same material, the optical term χ has a form[25,26]

$$\chi = \frac{2(\omega/c) N_z^{(nF)} N^{(0)} \cos\phi}{(N^{(0)}\cos\phi \mp N_z^{(nF)})(N^{(0)} N_z^{(nF)} \pm \varepsilon_0^{(nF)} \cos\phi)} \times \exp[-2iN_z^{(nF)}(\omega/c) t_1^{(nF)}], \tag{4}$$

where ϕ, ω, $N^{(0)}$, and $N^{(nF)} = \sqrt{\varepsilon_0^{(nF)}}$ are, respectively, the incidence angle, the angular frequency of the incident light, the complex refractive indices of air and of the non-FM (nF) sandwiching layers. The term $N_z^{(nF)} = \sqrt{N^{(nF)2} - N^{(0)2}\sin^2\phi}$ corresponds to the z component of the wave vector in the non-FM layers divided by the magnitude of the wave vector in vacuum, i.e., $N_z^{(nF)} = k_z^{(nF)}/k_0$. The influence of the thickness $t_1^{(nF)}$ of the non-FM cover layer is expressed by the exponential factor. The upper and lower signs in the denominator correspond to the s (Kerr s effect, $\Phi_s = -r_{ps}/r_{ss}$) and p polarized (Kerr p effect, $\Phi_p = r_{sp}/r_{pp}$) incident light, respectively, where the reflection coefficients r_{sp}, r_{ps} (r_{ss}, r_{pp}) are the off-diagonal (diagonal) elements of the Jones reflection matrix. If the non-FM substrate is finite, then the expression for the optical term χ is more complicated,[24] nevertheless the factorization in Eq. (3) is preserved.

The polar Kerr effect described by Eqs. (3) and (4) does not depend on the diagonal permittivity of the ultrathin FM layer $\varepsilon_0^{(F)}$. Consequently, the MO signal should not depend on its variation near the FM/non-FM interface. On the other hand, for ultrathin films, it is the off-diagonal permittivity $\varepsilon_1^{(F)}$ that contributes to the Kerr effect. Consequently, the Kerr effect depends on the variation of ε_1 across the FM layer. The details of this dependence and its variation with the shape of the ε_1 profile will be discussed in the following section.

III. INTERFACE CONTRIBUTIONS AND INTEGRAL OFF-DIAGONAL PERMITTIVITY EXCESS

The description of the FM/non-FM interface by a steplike profile of the off-diagonal permittivity is unsatisfactory to account for the nonzero Kerr effect extrapolation at zero FM layer thickness. For real interfaces it is possible to approximate the FM layer and its magneto-optically active surrounding by a stack of infinitesimally thin sublayers of thickness $t^{(i)}$ and constant off-diagonal permittivity $\varepsilon_1^{(i)}$. Due to its additive character,[28] the total Kerr effect of the stack of FM sublayers is a sum of the individual contributions from all these sublayers, i.e., $\Phi = \Sigma\Phi^{(i)} = \Sigma\chi^{(i)}\varepsilon_1^{(i)} t^{(i)}$. This situation is shown in Fig. 1. If the total thickness of all sublayers $\Sigma t^{(i)}$ satisfies the ultrathin approximation, the term $\chi^{(i)}$ is constant for all sublayers and will be noted by χ. Subsequently, the total Kerr effect can be expressed by

$$\Phi = \chi \sum_i \varepsilon_1^{(i)} t^{(i)} \equiv \chi \mathcal{E}. \tag{5}$$

As follows from the previous equation, the stack of discrete sublayers can be substituted by a continuous medium char-

acterized by an adapted profile $\varepsilon_1(\tau)$. Then, the expression of the Kerr effect can be written in the integral form

$$\Phi = \chi \int_{\text{MO active region}} \varepsilon_1(\tau) d\tau \equiv \chi \mathcal{E}. \tag{6}$$

The quantity $\mathcal{E}$ represents the total MO response of *all* magneto-optically active sublayers. This is why it has been defined as the *integral off-diagonal permittivity*.

Several types of off-diagonal permittivity profiles $\varepsilon_1(\tau)$ across the non-FM/FM/non-FM sandwich will be assumed. Depending on the level of simplification, they can be divided into three categories (Fig. 1).

(a) The first one corresponds to an ideal steplike profile. In this case the partial MO contributions are constant across the thickness of the FM film $t^{(\mathrm{F})}$ [Fig. 1(a)] and the total Kerr effect is expressed by $\Phi = \chi\mathcal{E} = \chi\varepsilon_1{}^{(\mathrm{F})} t^{(\mathrm{F})}$.

(b) In the second case, the profile of $\varepsilon_1(\tau)$ is assumed to be composed of three parts [Fig. 1(b)]. In the part 1, the value of $\varepsilon_1(\tau)$ is equal to the bulk value of the sandwiching non-FM layers, i.e., $\varepsilon_1(\tau) = \varepsilon_1^{(\mathrm{nF})} = 0$. In the part 2, $\varepsilon_1(\tau)$ is assumed to be equal to the bulk value $\varepsilon_1^{(\mathrm{F})}$ of the FM layer independently of the deposited thickness $t^{(\mathrm{F})}$. In part 3, which corresponds to the FM/non-FM interface region, the profile is quantified by some smooth function which is independent on $t^{(\mathrm{F})}$. Consequently, Eq. (6) leads to

$$\Phi = \chi\mathcal{E} = \chi(\mathcal{E}_A + \varepsilon_1^{(\mathrm{F})} t^{(\mathrm{F})}). \tag{7}$$

The quantity $\mathcal{E}_A$ introduced in Eq. (7) will be referred to as the *integral off-diagonal permittivity excess*, because it describes the difference between the integral off-diagonal permittivity of the real and steplike profiles, i.e.,

$$\mathcal{E}_A = \mathcal{E} - \varepsilon_1^{(\mathrm{F})} t^{(\mathrm{F})} = \int_{\text{MO active region}} \varepsilon_1(\tau) d\tau - \varepsilon_1^{(\mathrm{F})} t^{(\mathrm{F})}. \tag{8}$$

(c) In the third case, the off-diagonal permittivity $\varepsilon_1(\tau)$ is described by a general function of the position across the sandwich structure [see Fig. 1(c)]. In this case, the integral off-diagonal permittivity $\mathcal{E}$ is a general function of $t^{(\mathrm{F})}$. Although the function can have an arbitrary form, it can be approximated by an expression similar to Eq. (7), i.e.,

$$\mathcal{E}(t^{(\mathrm{F})}) = \int_{\text{MO active region}} \varepsilon_1(\tau, t^{(\mathrm{F})}) \mathrm{d}\tau \approx \mathcal{E}_A' + \varepsilon_1'^{(\mathrm{F})} t^{(\mathrm{F})}, \tag{9}$$

where $\varepsilon_1'^{(\mathrm{F})}$ and $\mathcal{E}_A'$ are some effective values of the off-diagonal permittivity and its corresponding integral excess.

In the following we will analyze category (b). For comparing the theoretical [expression (7)] and experimental [expression (1)] dependences of the Kerr effect on the FM layer thickness up to the linear term, it is convenient to use the ratio

$$\frac{A}{B} = \frac{\mathcal{E}_A}{\varepsilon_1^{(\mathrm{F})}}. \tag{10}$$

This expression shows that the experimentally deduced ratio A/B is directly related to the deviation of the integral off-diagonal permittivity (described by $\mathcal{E}_A$) from the ideal steplike permittivity profile. This is, therefore, the key point of the proposed method to analyze the MO interface contributions.

In the following, we will list theoretically predicted advantages of the A/B ratio.

(i) It is directly determined from the experimental FM thickness dependence of the Kerr effect.

(ii) From the definition of $\mathcal{E}_A$ given by expression (8) it follows that the A/B ratio is independent on the exact profile of the off-diagonal permittivity distribution $\varepsilon_1(\tau)$ across the interface regions. Its value is given by the difference between the integral off-diagonal permittivity of the real and steplike profiles, provided that the ultrathin approximation is fulfilled.

(iii) In the ultrathin approximation, this A/B ratio describes the MO properties of the FM/non-FM interface in a similar way as optical constants. It does *not* depend on the incidence angle and on the polarization of probing light. It is also invariant with respect to the other characteristics of the studied structures, such as the thickness and optical parameters of the non-FM sandwiching layers.

(iv) Although Eq. (10) was derived for a sandwich structure containing only a single ultrathin FM layer, it should be emphasized that it is also valid for systems with more *identical* ultrathin FM layers embedded in the same non-FM material, provided that the thickness of all the FM layers *together* fulfills the ultrathin approximation. We will show the derivation of this result for a structure consisting of two FM layers. Because of its additive character, the measured Kerr effect is a sum of contributions originating from both FM layers, i.e.,

$$\Phi = \Phi_1 + \Phi_2 = \chi_1\mathcal{E}_1 + \chi_2\mathcal{E}_2. \tag{11}$$

If the structure and magnetization states of both FM layers are identical, i.e., $\mathcal{E}_1 = \mathcal{E}_2 = \mathcal{E}$, the total Kerr effect can be factorized to a form consisting of the integral off-diagonal permittivity $\mathcal{E}$ and the effective optical term χ' given by the sum of the individual optical terms χ_1 and χ_2, i.e.,

$$\Phi = \chi'\mathcal{E}, \quad \chi' = \chi_1 + \chi_2. \tag{12}$$

From an experimental point of view, the dependence of the total Kerr effect on the FM layer thickness can be again described by an equation analogous to expression (1):

$$\Phi = A' + B' t^{(\mathrm{F})} + C' (t^{(\mathrm{F})})^2. \tag{13}$$

Here, $t^{(\mathrm{F})}$ stands for the thickness of the *single* FM layer embedded in the sandwich structure. Similarly as for Eq. (10), the comparison of expressions (12) and (13) results in the equality between the experimentally obtained value of A'/B' and the ratio $\mathcal{E}_A/\varepsilon_1^{(\mathrm{F})}$, where $\mathcal{E}_A$ is calculated as in expression (8).

(v) The approach described above can also be used for systems with ultrathin FM layers with in-plane magnetization. In this case, the off-diagonal permittivity is given by $\varepsilon_1^{(\mathrm{F})} = -i\varepsilon_{xz}^{(\mathrm{F})} = i\varepsilon_{zx}^{(\mathrm{F})}$. The longitudinal Kerr effect is proportional to the ratio between the off-diagonal and diagonal permittivities of the ultrathin FM film,[25] i.e.,

$$\Phi_{\text{long}} = \nu t^{(\text{F})} (\varepsilon_1^{(\text{F})} / \varepsilon_0^{(\text{F})}). \tag{14}$$

The optical term ν, which is the longitudinal analog of χ, is independent on the properties of the FM layer. Parameters equivalent to $\mathcal{E}$ and $\mathcal{E}_A$ can be defined in the longitudinal case by

$$\mathcal{E}_{\text{long}} = \int \frac{\varepsilon_1(\tau)}{\varepsilon_0(\tau)} d\tau,$$
$$\mathcal{E}_{A,\text{long}} = \int \frac{\varepsilon_1(\tau)}{\varepsilon_0(\tau)} d\tau - \frac{\varepsilon_1^{(\text{F})}}{\varepsilon_0^{(\text{F})}} t^{(\text{F})}. \tag{15}$$

The Kerr effect expresses as $\Phi_{\text{long}} = \nu \mathcal{E}_{\text{long}}$, and the ratio $(A/B)_{\text{long}}$ can be written as

$$\left(\frac{A}{B}\right)_{\text{long}} = \mathcal{E}_{A,\text{long}} \frac{\varepsilon_0^{(\text{F})}}{\varepsilon_1^{(\text{F})}}. \tag{16}$$

(vi) Expressions (6) and (8) show that the interface contribution to the total Kerr effect can be quantified by the integral off-diagonal permittivity excess $\mathcal{E}_A$. In order to include the interface contributions into the multilayer models[25,29], one can introduce ultrathin transition interface layers located between the FM and non-FM layers. These interface layers can be chosen arbitrarily. The only requirement is that they must include together the total integrated permittivity excess $\mathcal{E}_A$. It is, however, practical to use very simple layers. A good choice are two identical interface layers with the diagonal permittivity of the non-FM sandwiching layers. These interlayers have an equivalent thickness $t^{(\text{in})}$ [for example $t^{(\text{in})} = 1$ AL (atomic layer)] and are adjacent to the FM layer from both sides. For these interlayers, the off-diagonal permittivity $\varepsilon_1^{(\text{in})}$ differs from zero by a quantity

$$\Delta \varepsilon_1^{(\text{in})} = \frac{\mathcal{E}_A}{2t^{(\text{in})}}. \tag{17}$$

The factor 2 was used in the denominator to distribute the total excess between the two interface layers. Because the integral off-diagonal permittivity excess $\mathcal{E}_A$ is related to the ratio A/B through the expression (10), one obtains

$$\Delta \varepsilon_1^{(\text{in})} = \frac{\varepsilon_1^{(\text{F})}}{2t^{(\text{in})}} \frac{A}{B}. \tag{18}$$

With these interlayers one can reproduce the experimental data down to the limit of $t^{(\text{F})}$, when the part 2 in Fig. 1(b) disappears. Below this limit the model provides values $\Phi(t^{(\text{F})})$, which would be obtained from the experimental data by extrapolation. Note that $\Phi(t^{(\text{F})} = 0) = A$ for these interlayers.

IV. STUDIED SAMPLES AND EXPERIMENTAL PROCEDURES

In the following we apply the formal interface description developed above to analyze the polar Kerr effect data in Au/Co/Au(111) polycrystalline systems. In this section we shortly describe the preparation of samples and the experimental procedures used for the MO Kerr effect measurements. We report results on three different Au/Co specimens with stepped cobalt layers.

The samples were prepared by evaporation in ultra-high vacuum (10^{-10} Torr range). First, a 24-nm-thick Au(111) textured fcc polycrystalline buffer was prepared on a float glass substrate by room temperature deposition at a rate of 0.2 nm/s and subsequent annealing at 175 °C. The average crystallite size in the buffer layer was 100 nm, the atomically flat terraces with 30 nm average width were separated by monoatomic steps. An average r.m.s. roughness of the Au(111) surface measured by AFM over a $10\mu\text{m} \times 10\mu\text{m}$ area was about 0.5 nm (2.5 AL). This was confirmed by low-angle x-ray diffractometry on the entire surface of the sample.[30]

For two of the three specimens, 3 nm of Au was additionally deposited at room temperature onto the annealed buffer. This additional Au layer provides a long range smoothing of the surface, and suppresses in part the imperfections due to grain boundaries. Low-angle x-ray diffractometry showed that this additional Au layer has the same fcc crystallographic structure as the annealed buffer layer. The smoothing was confirmed by both RHEED and *in situ* resistivity measurements. However, we have not found any clear difference between the A/B ratios measured for specimens either covered or not by this additional Au layer.

On the high-quality Au(111) buffer layer the Co film was grown at room temperature at a deposition rate of 0.005 nm/s. Due to the large misfit between the Au and Co lattices (14%), the Co film grows initially in a double-layer mode. The Co film becomes continuous at $t^{(\text{Co})} = 2-3$ AL (0.4−0.6 nm). No variation of the Co surface roughness has been observed up to 15 AL (3 nm). These results are coherent with resistivity measurements on our samples during the Co film growth.[31] Furthermore, these results are consistent with previous STM studies[32] of the Co growth mode on a reconstructed Au(111) surface.

The Co film exhibits a (0001) hexagonal close-packed (hcp) structure, as checked on a few-nm-thick Co films by TEM and by ^{59}Co nuclear magnetic resonance.[31] 80–85 % of the Au-Co interface misfit is relaxed, while 20–15 % give strains.[33] Finally, the Co film was covered by an ultrathin gold overlayer, grown at room temperature at a deposition rate of 0.05 nm/s. The r.m.s. roughness of the top Au-Co interface is estimated to be 3 AL (0.6 nm), the Co crystallites having a mean size of about 7 nm.[30] These results agree with the data of cross section TEM of Au-Co interfaces.[34] Note that we previously evidenced a clear demixing between Au and Co.[35]

MO experiments were carried on the following three Au/Co structures with stepped cobalt layers. The first sample, indicated as *X*, has the following structure: Au(5 nm)/Co($t^{(\text{Co})}$)/Au(27 nm)/float glass substrate. The cobalt layer thicknesses are $t^{(\text{Co})} = 0.4, 0.6, 0.7, 0.8, \ldots,$ 1.5,1.6 nm. Each Co layer step has a width of 3 mm. The second sample *Y* is Au(7.5 nm)/Co($t^{(\text{Co})}$)/Au(28 nm)/float glass substrate. The cobalt layer thicknesses are here $t^{(\text{Co})}$

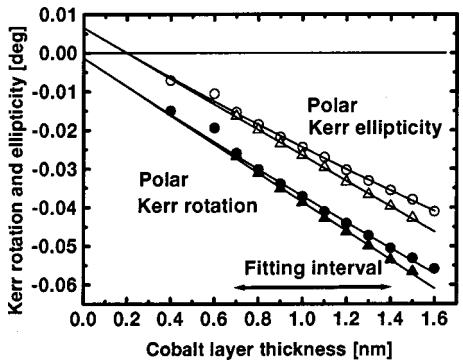

FIG. 2. Typical experimental variation of the polar Kerr rotation (solid symbols) and ellipticity (open symbols) with thickness of the Co layer in the sample *X*, measured at a photon energy of 3.45 eV at nearly normal incidence of light. The original experimental data for all thicknesses available for this sample are plotted by circles. The data used for the linear fitting procedure after subtraction of the nonlinear contributions, as described in the text, are plotted by triangles.

$=0.7$,0.8,0.9,1.0,1.1, and 1.2 nm, with a step width of 3 mm. The last sample *Z* considered here is a bilayer Au(5 nm)/Co($t^{(\mathrm{Co})}$)/Au(1.3 nm)/Co($t^{(\mathrm{Co})}$)/Au(27 nm)/float glass substrate. Both cobalt layers have the same thickness $t^{(\mathrm{Co})}=0.34$,0.7,0.9,1.1,1.3,1.5, and 1.9 nm. The individual step width is 4 mm. The samples *X* and *Z* were prepared exactly by the procedure mentioned above.

Sample *Y* was prepared in nearly the same way,[35] but without adding 3 nm of Au on the annealed Au buffer. This specimen was prepared in a different UHV chamber than *X* and *Z*.

Spectroscopic measurements of the polar Kerr effect have been performed by two equivalent methods, based on the modulation of the state of polarization of the light either by a Faraday cell with a feedback compensation[24,36] or by a photoelastic modulator.[23] The precision of both techniques is of the order of 10^{-4}deg.

The measurements were performed in the following geometries. For sample *X*, the Kerr *p* effect $\Phi_p=r_{sp}/r_{pp}$ was measured for incidence angles $\phi=7°$, 60°, and 80°. For sample *Y*, the angle of incidence was 5° (i.e., nearly normal incidence). For the bilayer *Z* the incidence angles were $\phi=7°$, 60°, 70°, and 80°, and for this sample both Kerr *s* effect ($\Phi_s=-r_{ps}/r_{ss}$) and Kerr *p* effect ($\Phi_p=r_{sp}/r_{pp}$) spectroscopic experiments were performed. The MO Kerr effect was measured in a magnetic field of 0.15 T after premagnetizing it at saturation with a pulse of 0.56 T applied during 1 s. The MO effect was deduced from the difference between MO signals for two opposite orientations of the magnetization vector.

A small Au diamagnetic contribution was measured separately on a part of the specimen with $t^{(\mathrm{Co})}=0$ nm and subtracted from the experimental Kerr effect for the nonzero $t^{(\mathrm{Co})}$ values. A typical variation of the Kerr rotation and ellipticity data with cobalt layer thickness $t^{(\mathrm{Co})}$ is shown in Fig. 2. The dependence on $t^{(\mathrm{Co})}$ can be described by the parabolic function [expression (1)]. As follows from the previous section, only the coefficients *A* and *B* are important. Therefore, in principle, to extract the coefficients *A* and *B*, it can be sufficient to fit the experimental data with the linear part of the expression (1).[20] Although this can be useful for a qualitative analysis, it is not sufficient for a more precise quantitative treatment. Inclusion of the nonlinearity associated with the coefficient *C* in expression (1) improves the accuracy on the values of the *A* and *B* coefficients, and it was therefore used in the data analysis.

The fitting procedure was carried out for cobalt layer thickness in the range of 0.7–1.4 nm, (3.5–7 AL). The surface morphology of the Co film does not change significantly on the considered thickness range. For thinner cobalt layers the experimental data exhibit quite large deviation from the expected ''smooth'' dependence of Φ on $t^{(\mathrm{Co})}$, as given by expression (1). As discussed above, this is related to the growth mode of the Co film. For Co layers thicker than 7 AL (1.4 nm), the magnetic anisotropy becomes not large enough to maintain an out-of-plane magnetization.[37] Then, for magnetic field values used in our experiments, the magnetic saturation is not reached. As a consequence, the Co films exhibit a smaller Kerr effect (a larger curvature in Fig. 2) than expected.

For present samples, the best fitting results were obtained when the nonlinear term $C(t^{(\mathrm{Co})})^2$ of expression (1) is calculated from the optical multilayer model.[29] For this calculation we used the optical data of Au (Ref. 20) and Co (Ref. 38) and the MO data of Co deduced from the experimental Kerr effect on thick Co films.[10] The coefficients *A* and *B* were then determined from the experimental data after subtracting the calculated nonlinear term $C(t^{(\mathrm{Co})})^2$. In other words, the data $\Phi-C(t^{(\mathrm{Co})})^2$ were fitted by the linear function $A+Bt^{(\mathrm{Co})}$.

V. EXPERIMENTAL RESULTS

In this section we show spectroscopic experimental data of interface contributions to MO polar Kerr effect in our Au/Co systems. These data are analyzed by using the method described in Sec. III.

Figure 3 shows typical experimental spectra of polar Kerr effect obtained for the sample *Z* with $t^{(\mathrm{Co})}=1.27$ nm. As expected, the spectra exhibit clear spectroscopic structures near 2.5 eV associated with the plasma edge in gold. This is a well-known effect induced by the optical properties of the buffer layer, which was discovered by Katayama *et al.* in the Fe/Cu system[39] in polar Kerr geometry. This effect was previously analyzed for the present Au/Co system in polar geometry.[20,24]

When the polar Kerr effect at (nearly) normal incidence is compared with the spectra of Φ_p and Φ_s for larger angles of incidence (e.g., for $\phi=70°$, as shown in Fig. 3), a significant qualitative difference is observed. Such a large difference results from the angular dependence of the Fresnel reflection coefficients especially in the vicinity of the principal angle of incidence. It should also be noted that the qualitative character of the Kerr spectra is independent on the cobalt layer thickness $t^{(\mathrm{Co})}$. We did not observe any clear features associated with the quantum well states in the Co layer, as already reported in other systems.[40] Note that the Au protective

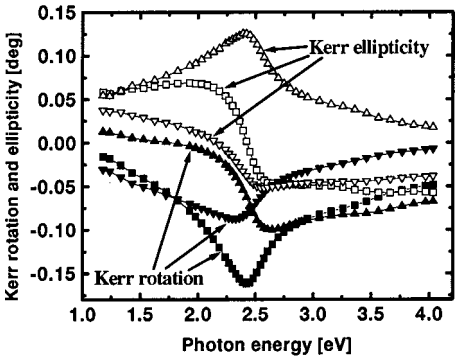

FIG. 3. Experimental spectra of the polar Kerr effect for the sample Z with two identical Co layers of thickness $t^{(\mathrm{Co})}=1.27$ nm. The spectra are represented for incidence angles $\phi=7°$ (squares) and $\phi=70°$, where the Kerr s effect Φ_s and the Kerr p effect Φ_p are displayed by triangles and inverted triangles, respectively.

layer is thick enough, so that the contributions to the Kerr effect due to the quantum well states in this layer can be neglected.[41]

A linear regression analysis of the polar Kerr effect variation with $t^{(\mathrm{Co})}$, performed after the subtraction of the quadratic contribution, provided spectra of the A and B coefficients as shown in Figs. 4(a) and 4(b). As expected from the theoretical analysis reported in Sec. III, the spectra of the A coefficient should vary significantly with the angle of incidence and with the polarization state of the incident light in the vicinity of the principal angle. This is due to the fact that A is proportional to χ, as it follows from the comparison of expressions (1) and (7). Indeed, such large variations are clearly observable in Fig. 4(a).

The spectra of the B coefficient have nearly the same shape as those of the polar Kerr effect in the same geometry. This is due to the fact that the term $Bt^{(\mathrm{Co})}$ in expression (1) is dominant in the expression of the Kerr effect.

Figure 5 shows the spectra of the ratio A/B determined from the analysis of the experimental data obtained on the bilayer Z for different angles of incidence ϕ and two incident polarizations. The larger experimental errors on the A/B ratio for larger photon energies are due to smaller absolute values of the A and B coefficients at these energies.

As can be seen from this figure, the ratio A/B exhibits only a weak (almost within the error bars) dependence on the angle of incidence ϕ, as predicted in Sec. III. On the other hand, the graphs demonstrate a slight difference between the values corresponding to the s and p polarized incident light; this difference is especially evident for photon energies higher than 3 eV.

In order to explain the origin of this difference, numerical analysis of the A/B ratio deduced from the Φ_p and Φ_s observables was performed. The experimental data were simulated by a model using the interface interlayers, as described in Sec. III. In the simulation, the polarization dependence of the A/B ratio was found to be much smaller than that shown in Fig. 5. This points out that the detected difference does not originate from the ultrathin approximation employed to analyze the data. Note that for this sample, the thickness of the Au interlayer separating the two Co layers is only 6.5 AL (1.3 nm); this approximately corresponds to the decay length of the oscillatory exchange coupling in the Au/Co/Au/Co/Au(111) system.[42] One can therefore expect that there will be still an appreciable MO Kerr contribution of the spin-polarized quantum well states in this Au layer[43,44] which can be sensitive to the incident polarization. Because we do not have a precise microscopic model of the interface, we cannot determine the origin of this difference. Another possible reason for this discrepancy could be a small systematic error between the experimental data measured for both polarizations.

Figure 6 compares the A/B ratios for the Au/Co interface contributions obtained for all studied samples. The resulting values are averages of all A/B ratios obtained for each individual specimen. Spectra of the ratios for all studied samples show very similar features. The A/B ratio exhibits a significant behavior near 2.5 eV, i.e., around the plasma edge of gold. This change is not an artifact of processing of the experimental Kerr effect spectra, which have a characteristic spectroscopic structure in this spectral region. It shows that the MO characteristics of the Au/Co interface are influenced

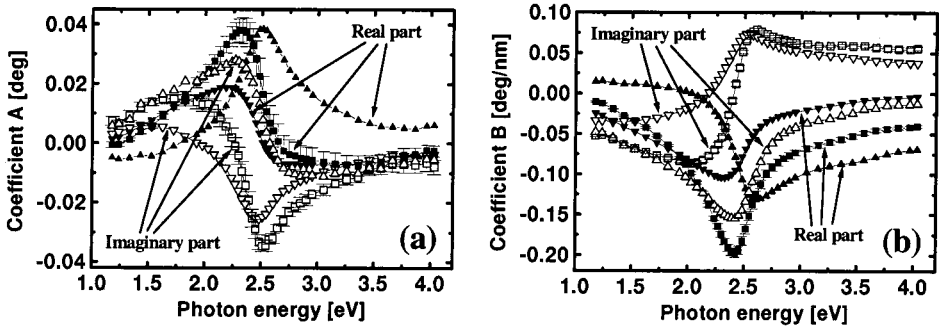

FIG. 4. Experimental spectra of the coefficients A (a) and B (b) obtained from the data of the polar Kerr effect measured on the specimen Z, examples of which are shown in Fig. 3. The spectra are displayed for the angles of incidence $\phi=7°$ (squares) and $\phi=70°$ (triangles for Φ_s and inverted triangles for Φ_p). The typical error bars are shown for the angle of incidence $\phi=7°$ and correspond to the standard deviation of the linear fit, as described in Sec. IV. The error bars for the other curves have similar magnitude and were omitted.

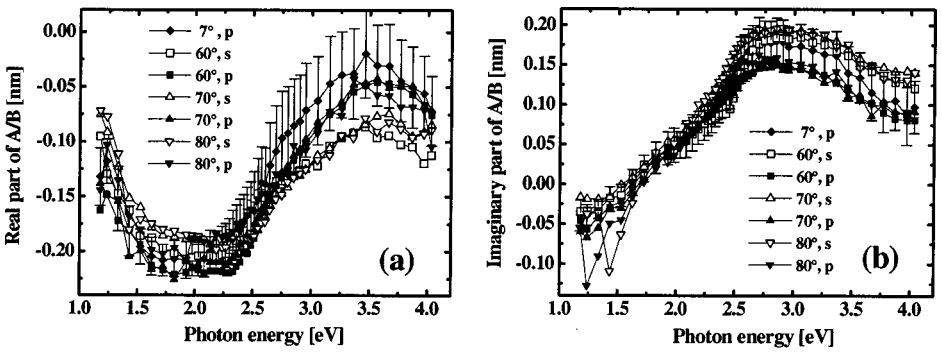

FIG. 5. Experimental values of the A/B ratio obtained from the Kerr s effect Φ_s (empty symbols), the Kerr p effect Φ_p (filled symbols) measured on the sample Z at different angles of incidence. The error bars display typical standard deviations, as obtained from the linear regression procedure described in Sec. IV.

by a microscopic mechanism related to the optical properties of gold.

It should be emphasized that the Fig. 6 contains valuable experimental results. These can be compared with theoretical calculations which provide the complex MO observables, i.e., the Kerr rotation and ellipticity. To obtain the A/B ratio, it is only necessary to consider a similar procedure to that used for the treatment of our experimental data.

Figure 7 shows the spectral variation of the quantity $\Delta\varepsilon_1^{(\mathrm{in})}$ defined in expression (17), as obtained from the experimental data of A/B by expression (18). In the calculation, one assumed $t^{(\mathrm{in})}=1$ AL (0.2 nm). The off-diagonal permittivity of the cobalt layer was calculated from the polar Kerr effect spectra of a thick Co film[10] using known optical indices.[38]

VI. MODELING OF THE Au/Co INTERFACE

We have already separated the contribution of the FM/non-FM interfaces from the total Kerr effect. Let us now discuss its possible origins. As mentioned in the Introduction, there are several effects which can be responsible for the interface MO contributions. The most interesting one is that related to the hybridization of the electronic wave functions of neighboring Au and Co monoatomic layers at the Au/Co interface.[20] In a simple macroscopic formalism one of course cannot evaluate this interface contribution. From the theoretical side, and to our knowledge, up to now there is no available *ab initio* calculation of the effect of the Co/Au interface hybridization on optical properties. Other possible mechanisms can also contribute to the interface MO term in real samples and that cannot be *a priori* neglected. In this section it will be shown how some of the contributions of these mechanisms can be included in the general formalism and compared with the experimental data of the A/B ratio (Fig. 8).

A. Disorder at the interface

It is well known that Co and Au do not intermix together (Sec. IV or Ref. 35). Thus, from the structural point of view only the interface roughness has to be considered. Recall that Co grows on large Au buffer atomically flat terraces with typical size of 30 nm, and forms first 2 AL thick islands. For a Co coverage larger than 2 AL, the islands tend to coalesce and form a continuous film with a textured polycrystalline structure giving local peak-to-peak roughness estimated to be about 2 AL. That is why there is a significant difference between the nature of the two involved Au/Co interfaces. The top one is locally more perturbed than the first one, which can be assumed flat over short distances. Suppressing the local roughness, a longer range roughness having a rms value of 3 AL still contributes as due to Au grain boundaries and other defects.

In the absence of a universal optical and MO theory in the presence of rough interfaces, we shall consider a simple interpretation of the data. In order to model the disorder at both interfaces, we shall distinguish between short and long range roughnesses. The short range roughness takes place at the range of few atomic distances. It is justified that short range roughness can be modeled in the framework of the Bruggeman effective medium approximation (EMA).[45,46] In spite of its different origin, the calculation will be the same as for real Co-Au intermixing. In counterpart, the longer range Co thickness variations may be estimated independently. As discussed above, the short range roughness contribution origi-

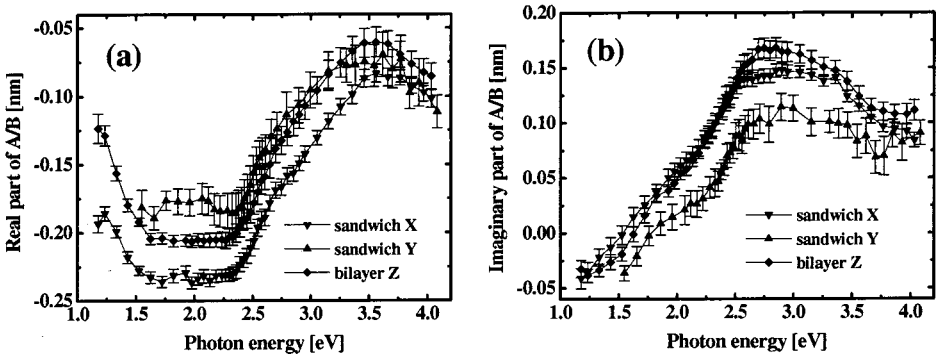

FIG. 6. Real (a) and imaginary (b) parts of the experimental ratio A/B for all three studied Au/Co specimens. Each curve was obtained as an average of all experimental spectra of the A/B ratio available for each specimen.

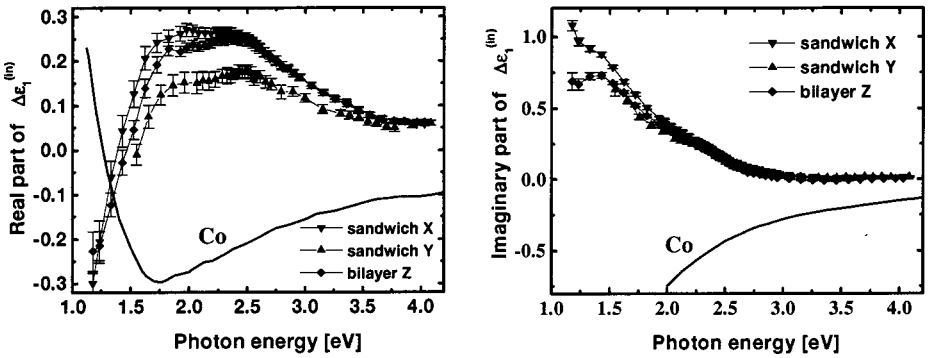

FIG. 7. Real (a) and imaginary (b) parts of the quantity $\Delta\varepsilon_1^{(\mathrm{in})}$ acquired from all studied Au/Co structures. They are compared with the bulk values of the off-diagonal permittivity of cobalt (solid lines). The Au/Co interface interlayer was assumed to have thickness $t^{(\mathrm{in})}=1$ AL (0.2 nm).

nates only from the upper Au/Co interface. The long range contribution accounts for both interfaces through the spatial variation of the Co layer thickness. The thickness variation of the Au overlayer and the roughness of the air/Au interface give negligible MO contributions.

1. Short range roughness

Consider the first contribution of interface disorder that comes from short range roughness. This contribution can be described within the EMA. Let the parameter x be a volume ratio of cobalt in the mixture. Then $\Delta\varepsilon_1^{(\mathrm{in})}=\varepsilon_1^{(\mathrm{mix})}-x\varepsilon_1^{(\mathrm{F})}$ and by using Eq. (18) the A/B ratio can be expressed as

$$\left(\frac{A}{B}\right)_{\mathrm{mix}}=2t^{(\mathrm{in})}\left(\frac{\varepsilon_1^{(\mathrm{mix})}}{\varepsilon_1^{(\mathrm{F})}}-x\right), \tag{19}$$

where $\varepsilon_1^{(\mathrm{mix})}$ is the off-diagonal permittivity of the mixture.

The short range roughness effect was calculated assuming an interface thickness $t^{(\mathrm{in})}=2$ AL (0.4 nm) that corresponds to the local peak to peak roughness of the upper Au/Co interface. The MO effects due to this contribution are depicted in Fig. 8, assuming a hypothetical $Au_{0.5}Co_{0.5}$ interface layer. When changing interlayer concentration by $\pm 20\%$, the spectral variation of the A/B ratio does not change significantly. The calculated spectral variation of the A/B ratio has some similarities to the experimental data, but its magnitude is smaller than that observed. Thus, this contribution alone is unable to explain the main part of the interface MO contribution.

2. Variation of Co layer thickness due to roughness

The most important effect due to the long range roughness is related to the variation of the Co layer thickness. This model assumes that the interfaces of the Co layer are not ideally flat, but consist of flat areas (terraces) separated by steps. As a result, the thicknesses of the Co film change along the specimen. In our case, the terraces are quite large (tens of nanometers), but are much shorter than the light wavelength. Then, the specimen could be modeled as an assembly of close microscopic structures with different Co thickness.

The distribution $g^{(i)}$ of cobalt layer thickness is determined by a mean value of cobalt thickness $t^{(F)}=\Sigma t^{(i)}g^{(i)}$ and by its variation $\sigma^{(F)}=[\Sigma g^{(i)}(t^{(i)}-t^{(F)})^2]^{1/2}$. The Kerr effect in such a system can be computed as a ratio of reflection coefficients ($\Phi_s=-r_{sp}/r_{ss}, \Phi_p=r_{ps}/r_{pp}$). These macroscopic reflection coefficients were determined as a weighted average of the reflection coefficients which were calculated for different cobalt layer thicknesses $r_{uv}=\Sigma g^{(i)}r_{uv}^{(i)}$ (the subscripts u, v stand for s or p polarization). The dependence of the A term (or the A/B ratio) on total roughness is quadratic ($A\sim\sigma^{(F)2}$).[47] On one hand, if both Au/Co interfaces display uncorrelated roughness σ_1 and σ_2, then the Co layer thickness variation is $\sigma^{(F)}=(\sigma_1^2+\sigma_2^2)^{1/2}$. On the other hand, if both interfaces have identical and fully correlated roughness, then $\sigma^{(F)}=0$. The quadratic increase of this contribution with $\sigma^{(F)}$ is obvious because the linear terms cancel after averaging. This mechanism therefore falls beyond the ultrathin linear approximation.

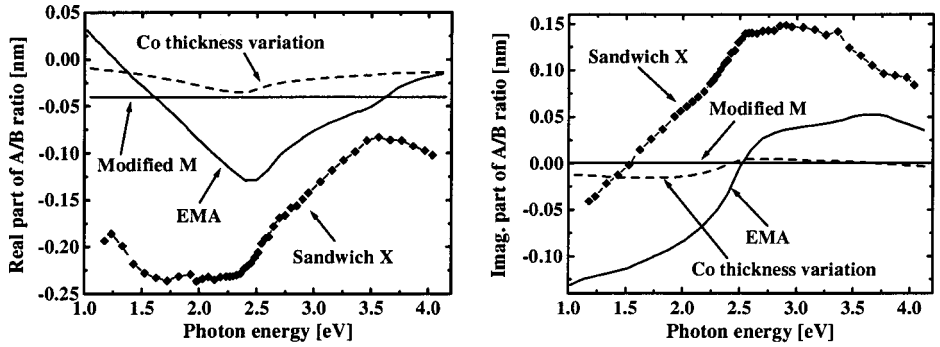

FIG. 8. Real (a) and imaginary (b) parts of the A/B ratio calculated for (i) the short range roughness of the Co layer surface (over the thickness $t^{(\mathrm{in})}=0.4$ nm) computed by using the effective medium approximation (EMA), (ii) the contribution of Co thickness variation $\sigma^{(F)}=0.6$ nm, and (iii) the modified magnetic moment $m=0.9$ of one Co monolayer of thickness $t^{(\mathrm{in})}=0.2$ nm.

In principle, there could be also long range surface roughness contributions of the Au buffer and overlayer. These effects were evaluated and found to be negligible (1% of the contribution of the Co thickness variation).

Both Au/Co interfaces exhibit long-range r.m.s. roughness of about 3 AL. However, we can assume that they are partly correlated. We estimate that the maximum peak to peak Co terraces thickness variation is not larger than $\sigma^{(F)}=3$ AL (0.6 nm). This ''long range roughness'' contribution to the A/B ratio is plotted in Fig. 8 for a Au(5 nm)/Co($t^{(\mathrm{Co})}$)/Au film. The shape of the calculated A/B spectra is close to that calculated by EMA. As it is seen in Fig. 8, this last mechanism contributes much less than the previous ''short range roughness'' term.

B. Modified magnetic moment of Co atoms at the interface

This model assumes that the cobalt atoms which are in contact with the gold layer have magnetic moment different from those in the inner part of the Co film. This can be accounted for by considering that a part of the Co layer, with thickness $t^{(\mathrm{in})}$, has a relative magnetization $m\neq 1$. Consequently, $\Delta\varepsilon_1^{(\mathrm{in})}=(m-1)\varepsilon_1^{(\mathrm{Co})}$ and Eq. (18) implies that

$$\left(\frac{A}{B}\right)_{\mathrm{Co}}=2(m-1)t^{(\mathrm{in})}. \tag{20}$$

As is immediately seen from expression (20), this contribution is invariant with respect to the photon energy and affects only the real part of the A/B ratio. The Fig. 8 presents this contribution for one monolayer of Co atoms ($t^{(\mathrm{in})}=0.2$ nm) with a reasonable reduction of the magnetic moment by 10% ($m=0.9$) at the Au/Co interface. Because this contribution is a real number, it cannot account for the imaginary part of the A/B ratio and the spectral variation of the data. This mechanism would have only a tiny effect.

C. Au-Co electronic hybridization

In order to describe the observed MO contribution of the Au/Co interfaces it is necessary to change the off-diagonal permittivity of one monoatomic interface layer by a value which is of the same order of magnitude as the off-diagonal permittivity of cobalt $\varepsilon_1^{(\mathrm{Co})}$. The modified magnetization at the interface and the changes of $t^{(\mathrm{Co})}$ along the specimen due to the interface roughness are too small to explain the experimental interface contributions in the Au/Co system. The contribution of the effective top Au-Co interlayer calculated in the effective medium approximation (EMA) also does not describe the observed A/B ratio satisfactorily. Therefore, our results suggest that the most important part of the interface contribution arises from intrinsic properties of the interface itself, i.e., from the Au-Co electronic hybridization.

The experimental data interpreted through macroscopic models involving different contributions to the interface-related MO signals should provide useful material to be compared with results of *ab initio* calculations of layer-resolved permittivity tensor.[16] The suggested representation of interface effects by integral permittivity excess is very general and can be compared with any type of the permittivity tensor profile determined theoretically.

It would be very useful to extract the net contribution of electronic interface hybridization from the experimental data. This should be possible for systems where the film grows pseudomorphically layer by layer, giving rise to very flat FM/non-FM interfaces. In such a case the presence of interlayers, described within the EMA, can be excluded. Then, real space studies of surface morphology would provide structural parameters to account for roughness effects and the intrinsic electronic contribution would be determined.

In the case of Au/Co/Au(111) structures the situation is somewhat more complicated. Although the bottom interface of Co layer is planar at the microscopic scale, the top Au/Co interface has a complex topology determined by the structure of the Co film surface. This will, to some extent, affect the electronic interaction at the top interface, because the configuration of the nearest neighbors will not be uniform along the interface plane. Consequently, the electronic contribution will also depend on geometry of this interface. Therefore it will not be possible to separate *exactly* the contribution of effective intermixing from that due to electronic hybridization at the flat Au/Co interface. We believe, that this problem is not too serious because the lower interface is flat on a nanometer scale. The top Au/Co interface is also reasonably flat on the surface of Co islands. Therefore, in our opinion, the approximate separation of these two contributions is certainly valid and the present experimental data of interface MO contributions may be compared with *ab initio* calculations of the effect of electronic hybridization at flat Au(111)/Co interfaces.

VII. CONCLUSION

By using analytical expressions of the MO Kerr effect in simple structures with ultrathin magnetic layers, we developed an original procedure to extract the magneto-optical parameters of interfaces between ferromagnetic and nonferromagnetic metals. The interface contributions were expressed as a ratio A/B of coefficients describing the experimental variation of the complex Kerr effect with thickness of the ferromagnetic film $t^{(\mathrm{F})}$, using a linear approximation $\Phi\approx A+Bt^{(\mathrm{F})}$. The advantage of this representation is that the A/B ratio is independent on experimental conditions (i.e., the angle of incidence and the polarization state of the incident light), as well as on the optical properties and thicknesses of sandwiching layers.

The procedure allows one to extract the interface-related information from standard MO experiments. It also provides more reliable physical data relevant to the interface-induced contributions to the MO observables. This kind of analysis allows to link the experimental studies to the theoretical calculations of electronic interactions at the FM/non-FM interfaces.

This treatment was applied to three Au/Co/Au(111) polycrystalline structures with perpendicular magnetic anisotropy. The interface contributions were analyzed by measuring the MO Kerr effect at different angles of incidence on different specimens. The experimental results have con-

firmed the advantages of the proposed procedure in the treatment of the data on interface MO contributions. These results also prove that the interface effects can be accounted for by macroscopic optical approaches and described by a variation of the local optical permittivity tensor in the interface regions. The off-diagonal permittivity excess $\Delta\varepsilon_1^{(\mathrm{in})}$ can be calculated directly from the experimental value of the A/B ratio under condition that the off-diagonal permittivity of the inner part of the FM layer is known.

The effect of several processes, which could be partially responsible for the interface contributions in non-FM/FM/non-FM systems, was estimated by using simple models. Models taking into account the short range film roughness and the variation of Co layer thickness provide interface contributions which have spectroscopic features similar to the experimental data. However, to agree with calculations, one would have to consider much larger roughness of the interfaces than that measured. Thus, such structural effects cannot explain the too large magnitude of the MO interface effects. Therefore, another contribution has to be considered. We suggest that this comes from the Au-Co electronic hybridization at the Au/Co interfaces. *Ab initio* calculations of the layer-resolved permittivity tensor are needed to provide deeper understanding of this problem.

ACKNOWLEDGMENTS

The authors acknowledge Mme. M. Galtier for preparing some of the samples and J. Mistrík and A. Mougin for critical readings of the manuscript. This work was partially sponsored by the Grant Agency of The Czech Republic (Grant No. 220/97/1180, 202/00/0761, and 202/99/D060). One of the authors (J.H.) would also like to thank the Laboratoire de Physique des Solides, Université Paris-Sud, Orsay for its kind hospitality during his stays, and the Ministère des affaires étrangères for financial support. Another author (M.N.) also acknowledges the Max-Planck-Institut für Mikrostrukturphysik in Halle for a friendly and stimulating atmosphere and for a financial support during final stages of this work.

*On leave at: Max-Planck-Institut für Mikrostrukturphysik, Weinberg 2, 06120 Halle, Germany

†Corresponding author: ferre@lps.u-psud.fr

[1] U. Gradmann, J. Magn. Magn. Mater. **54-57**, 733 (1986).

[2] N.C. Koon, B.T. Jonker, F.A. Volkening, J.J. Krebs, and G.A. Prinz, Phys. Rev. Lett. **59**, 2463 (1987).

[3] C. Chappert and P. Bruno, J. Appl. Phys. **64**, 5736 (1988).

[4] C. Liu, E.R. Moog, and S.D. Bader, Phys. Rev. Lett. **60**, 2422 (1988).

[5] M. Mansuripur, *The Physical Principles of Magneto-optical Recording* (Cambridge University Press, Cambridge, 1998).

[6] J.C.S. Kools, IEEE Trans. Magn. **32**, 3165 (1996).

[7] S. Tehrani, J.M. Slaughter, E. Chen, M. Durlam, J. Shi, and M. DeHerrera, IEEE Trans. Magn. **35**, 2814 (1999).

[8] S. D. Bader and J. Erskine, in *Ultrathin Magnetic Structures II*, edited by B. Heinrich and J. A. C. Bland (Springer-Verlag, Berlin, 1994).

[9] W.B. Zeper, F.J.A.M. Greidanus, P.F. Carcia, and C.R. Fincher, J. Appl. Phys. **65**, 4971 (1989).

[10] H. Brändle, D. Weller, J.C. Scott, S.S.P. Parkin, and C.-J. Lin, IEEE Trans. Magn. **28**, 2967 (1992).

[11] D. Weller, H. Brändle, and C. Chappert, J. Magn. Magn. Mater. **121**, 461 (1993).

[12] Š. Višňovský, M. Nývlt, V. Parízek, P. Kielar, V. Prosser, and R. Krishnan, IEEE Trans. Magn. **29**, 3390 (1993).

[13] S. Uba, L. Uba, A.N. Yaresko, A.Y. Perlov, V.N. Antonov, and R. Gontarz, J. Phys.: Condens. Matter **9**, 447 (1997).

[14] S. Uba, A.N. Yaresko, L. Uba, A.Y. Perlov, V.N. Antonov, R. Gontarz, and H. Ebert, Phys. Rev. B **57**, 1534 (1998).

[15] K. Sato, E. Takeda, M. Akita, M. Yamaguchi, K. Takanashi, S. Mitani, H. Fujimori, and Y. Suzuki, J. Appl. Phys. **86**, 4985 (1999).

[16] T. Huhne and H. Ebert, Phys. Rev. B **60**, 12 982 (1999).

[17] W. Weber, C. H. Back, A. Bischof, C. Würsch, and R. Allenspach, Phys. Rev. Lett. **76**, 1940 (1996).

[18] P. Bruno, Y. Suzuki, and C. Chappert, Phys. Rev. B **53**, 9214 (1996).

[19] Y. Suzuki, T. Katayama, P. Bruno, S. Yuasa, and E. Tamura, Phys. Rev. Lett. **80**, 5200 (1998).

[20] Š. Višňovský, M. Nývlt, V. Prosser, J. Ferré, G. Pénissard, D. Renard, and G. Sczigel, J. Magn. Magn. Mater. **128**, 179 (1993).

[21] S.T. Purcell, M.T. Johnson, N.W.E. McGee, J.J. de Vries, W.B. Zeper, and W. Hoving, J. Appl. Phys. **73**, 1360 (1993).

[22] N.W.E. McGee, M.T. Johnson, J.J. de Vries, and J. aan de Stegge, J. Appl. Phys. **73**, 3418 (1993).

[23] C. Train, P. Beauvillain, V. Mathet, G. Pénissard, and P. Veillet, J. Appl. Phys. **86**, 3165 (1999).

[24] Š. Višňovský, M. Nývlt, V. Prosser, R. Lopušník, R. Urban, J. Ferré, G. Pénissard, D. Renard, and R. Krishnan, Phys. Rev. B **52**, 1090 (1995).

[25] Š. Višňovský, Czech. J. Phys., Sect. B **48**, 1083 (1998).

[26] A. Hubert and G. Traeger, J. Magn. Magn. Mater. **124**, 185 (1993).

[27] V. Kamberský, L. Wenzel, and A. Hubert, J. Magn. Magn. Mater. **189**, 149 (1998).

[28] J. Zak, E.R. Moog, C. Liu, and S.D. Bader, J. Magn. Magn. Mater. **88**, L261 (1990).

[29] Š. Višňovský, Czech. J. Phys., Sect. B **36**, 625 (1986).

[30] C. Marlière, D. Renard, and J.-P. Chauvineau, Thin Solid Films **201**, 317 (1991).

[31] J. Corno, M. Galtier, D. Renard, J.P. Renard, and F. Trigui, Eur. Phys. J. B **10**, 223 (1999).

[32] B. Voigtländer, G. Meyer, and N.M. Amer, Phys. Rev. B **44**, 10 354 (1991).

[33] F. Hakkens, A. De Veirman, W. Coene, and F. den Broeder, J. Mater. Res. **8**, 1019 (1993).

[34] N. Mliki, K. Abdelmoula, C. Leroux, and G. Nihoul, Philos. Mag. B **71**, 913 (1995).

[35] C. Train, M. Nývlt, B. Bartenlian, P. Beauvillain, V. Mathet, R. Mégy, and Š. Višňovský, J. Magn. Magn. Mater. **165**, 417 (1997).

[36] M. Nývlt, PhD. dissertation, Charles University, Prague, 1996.

[37] V. Grolier, J. Ferré, A. Maziewski, E. Stefanowicz, and D. Renard, J. Appl. Phys. **73**, 5939 (1993).

[38] P.B. Johnson and R.W. Christy, Phys. Rev. B **9**, 5056 (1974).
[39] T. Katayama, Y. Suzuki, H. Awano, Y. Nishihara, and N. Koshizuka, Phys. Rev. Lett. **60**, 1426 (1988).
[40] W. Geerts, Y. Suzuki, T. Katayama, K. Tanaka, K. Ando, and S. Yoshida, Phys. Rev. B **50**, 12 581 (1994).
[41] R. Mégy, A. Bounouh, Y. Suzuki, P. Beauvillain, P. Bruno, C. Chappert, B. Lecuyer, and P. Veillet, Phys. Rev. B **51**, 5586 (1995).
[42] V. Grolier, D. Renard, B. Bartenlian, P. Beauvillain, C. Chappert, C. Dupas, J. Ferré, M. Galtier, E. Kolb, M. Mulloy, J. P. Renard, and P. Veillet, Phys. Rev. Lett. **71**, 3023 (1993).
[43] W.R. Bennett, W. Schwarzacher, and W.F. Egelhoff, Jr., Phys. Rev. Lett. **65**, 3169 (1990).
[44] M. Nývlt, Š. Višňovský, J. Ferré, D. Renard, and M. Galtier (unpublished).
[45] D. E. Aspnes, in *Handbook of Optical Constants of Solid*, edited by E. D. Palik (Academic Press Handbook Series, London, 1985).
[46] M. Abe and M. Gomi, Jpn. J. Appl. Phys. **23**, 1580 (1984).
[47] R. Urban, M. Nývlt, Š. Višňovský, J. Ferré, D. Renard, M. Galtier, and P. Beauvillain, J. Magn. Soc. Jpn. **22**, Suppl. S2 197 (1998).